Fast Antenna and Beam Switching Method for mmWave Handsets with Multiple Subarrays

Wan-Ting Shih[‡], Chao-Kai Wen[†], Shi Jin[♮], and Shang-Ho Tsai[*]
[‡]Institute of Electrical and Control Engineering, National Chiao Tung University
Hsinchu 300, Taiwan, Email: sydney2317076@gmail.com
[†]Institute of Communications Engineering, National Sun Yat-sen University
Kaohsiung 804, Taiwan, Email: chaokai.wen@mail.nsysu.edu.tw
[♮]National Mobile Communications Research Laboratory, Southeast University
Nanjin 210096, P. R. China, Email: jinshi@seu.edu.cn
[*]Department of Electrical Engineering, National Chiao Tung University
Hsinchu 300, Taiwan, Email: shanghot@mail.nctu.edu.tw

***Abstract*—Millimeter-wave (mmWave) communication has become a promising option for meeting the multi-fold increase in demand for mobile data in the fifth-generation (5G) mobile broadband. However, when mmWave is applied to a mobile terminal device, communication can be frequently broken due to rampant hand blockage. Although this problem can be overcome by configuring multiple sets of subarrays at different locations, developing a fast and efficient operation that can find the best subarray and beam direction with power, complexity, and latency constraints is extremely challenging. In this study, we propose a fast antenna and beam switching method termed 'Fast-ABS' that uses only one antenna module for the reception to predict the best beam of other subarrays. Through extensive simulations, we demonstrate that Fast-ABS achieves efficient and seamless connectivity under hand blockage. In addition, we implement Fast-ABS on software radios and integrate it into the 5G New Radio physical layer. Our experiments show that the performance of the proposed beam switching method is close to that of an "Oracle" solution that can instantaneously identify the best beam of other subarrays even in complex non-line-of-sight scenarios.**

***Index Terms*—mmWave, multiple antenna modules, beam switching**

I. Introduction

With the congestion of the microwave frequency band, millimeter-wave (mmWave) communication is emerging as a promising solution to meet the multi-fold increase in demand for mobile data. mmWave communication has been reorganized as a key technology for fifth-generation (5G) mobile networks and beyond. Given that mmWave signals suffer from severe path-loss, mmWave devices should use array antennas to focus their radio frequency (RF) energy through narrow directional beams and compensate for attenuation loss. However, aligning beams between a base station (BS) and user equipments remains a fundamental challenge due to the high channel dynamics in device mobility, obstacle blockage, and the large number of possible beam directions.

When using a mobile phone, the user's fingers frequently hold the phone, shielding the mmWave antenna array and failing to receive signals. A number of mobile phone companies, e.g., [1–3], have proposed to configure multiple sets of mmWave antenna modules on mobile phones to overcome this problem. As shown in Fig. 1, unmasked subarrays can be selected for switching to avoid the problem of poor quality or disconnection of mmWave communication due to the shielding of the subarray that is being used. Identifying the optimal array antenna and beam direction by simultaneously enabling multiple sets of subarrays causes the problem of excessive power consumption and device costs. In general, one RF chain is a reasonable architecture for an initial generation of mmWave mobile phones [4]. Therefore, developing an effective switching antenna mechanism that can maintain the communication performance of mobile phones becomes a critical task.

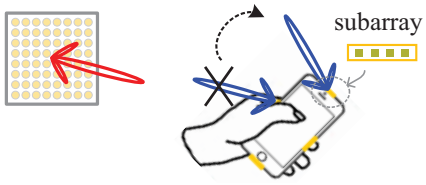

Fig. 1. Avoiding hand blockage by switching antenna modules and beams.

In [4] and [5], the researchers suggested switching to another subarray in turn and re-scanning the best beam direction, i.e., re-processing the initial access [6], for the reception when an object blocks the received subarray. This approach can require a long latency period to find the best subarray and build beam alignment. In [7], the authors proposed to use knowledge of the user's hand grip of a mobile phone (e.g., when browsing or taking photos) to switch antennas and design corresponding codebooks to reduce the number of searches. However, this method requires knowing the usage mode information of mobile phones, and the performance still depends on the size of searches.

In this study, we propose a fast antenna and beam switching method, referred to as Fast-ABS, for mmWave handsets with multiple subarrays. Our method is basically built upon two observations.

First, although the steering vector changes with different subarrays and orientations, the underlying physical paths of the signals propagating from the transmitter to the compact receiver remain unchanged in free space. Therefore, if one subarray can extract

The work of W.-T. Shih and C.-K. Wen was supported in part by the Ministry of Science and Technology of Taiwan under grants MOST 108-2218-E-110-014- and MOST 108-2221-E-110-010-MY2.

The work of S. Jin was supported in part by the National Science Foundation (NSFC) for Distinguished Young Scholars of China with Grant 61625106.

978-1-7281-5089-5/20/$31.00 ©2020 IEEE

Authorized licensed use limited to: National Chiao Tung Univ.. Downloaded on April 26,2022 at 10:09:46 UTC from IEEE Xplore. Restrictions apply.

the properties (i.e., complex gain and directionality) of the paths, then the channel spatial information of the other subarrays can be reconstructed without scanning all the subarrays.

Second, although the underlying propagation paths for a blocked subarray can be complex due to the coupling and reflection caused by the user's fingers, their detailed properties are irrelevant because using a blocked subarray should be avoided. Only a simple power detector is required to detect whether a subarray is experiencing hand blockage.

By extracting the properties of the paths from one receiver subarray, along with the power information of other subarrays, all the beam directions from all the subarrays can be ranked in a user's handset by using only the current subarray's channel measurement. To achieve the goal of the first observation, we also propose to infer the relevant properties, i.e., complex gains and angle of arrival (AoA), of dominant paths by utilizing beam-specific channel impulse responses measured under different beams. The simulation results show that only three to four probings are required to infer the relevant properties. Moreover, we implement and evaluate Fast-ABS in a 5G New Radio (NR) device that supports two subarrays in various static and dynamic settings. Our experiments show that the signal-to-noise ratio (SNR) under Fast-ABS is close to that under optimal beam by exhaustive search.

II. Background of 5G mmWave

In the operation of 5G NR at mmWave, a pair of beams should be initially established in the downlink and uplink transmission directions. To achieve this object, a mobile device must acquire a synchronization signal block (SSB) transmitted from a BS by using different receiver beams. We consider an analog-based receiver-side beam-forming technique, wherein a receiver beam can only focus in one direction at a time. In particular, the receiver is equipped with a set of uniform linear arrays, and each array has N antenna elements with a uniform separation d. Given the analog weights $\{w_m(n), n = 0, \ldots, N-1\}$ of the m-th beam, the corresponding gain pattern can be expressed as

$$A_m(\theta) = \sum_{n=0}^{N-1} w_m(n) e^{-j2\pi n \frac{d\cos\theta}{\lambda}}, \tag{1}$$

where λ is the wavelength of the wireless signal. Thus, the mmWave channel created by the m-th receiver beam is given by

$$h_m(t) = \sum_{l=1}^{L} g_l \cdot A_m(\theta_l) \cdot \delta(t - \tau_l), \tag{2}$$

where L is the number of multiple paths; and g_l, τ_l, and θ_l denote the complex channel gain, AoA, and time of arrival (ToA) of the l-th path, respectively. Here, $A_m(\theta_l)$ represents the (beamforming) gain along direction θ_l when the receiver uses the m-th beam. The analog weights $w_m(n)$ can be transformed to generate different beams that correspond to desired directions.

Subsequently, the selection of the transmitter-side or receiver-side beam directions should be reevaluated regularly due to the movements and rotations of a mobile device. To facilitate this process, the BS transmits within the same beam, and then the mobile device performs receiver-side beam sweeping to measure the configured state information channel state information reference signal (CSI-RS) in sequence over a set of receiver beams. The 5G NR system is operated via orthogonal frequency-division multiplexing (OFDM). The aforementioned measurements can be performed on a configured CSI-RS in the frequency domain. The channel response of (2) in the frequency domain is given by

$$H_m[f_n] = \sum_{l=1}^{L} g_l \cdot A_m(\theta_l) \cdot e^{-j2\pi\tau_l f_n}, \tag{3}$$

where f_n is the n-th sub-carrier frequency. We can estimate $\{H_m[f_n]\}$ by dividing subcarrier outputs by the known RS at subcarriers $\{f_1, f_2, \cdots, f_{N_s}\}$.

Over a set of receiver beams $\mathcal{M} = \{m_1, m_2, \cdots, m_{M_s}\}$, the receiver can obtain a CSI matrix as follows:

$$\mathbf{H} = \begin{bmatrix} H_{m_1}[f_1] & H_{m_1}[f_2] & \cdots & H_{m_1}[f_{N_s}] \\ \vdots & & \ddots & \\ H_{m_{M_s}}[f_1] & H_{m_{M_s}}[f_2] & \cdots & H_{m_{M_s}}[f_{N_s}] \end{bmatrix}. \tag{4}$$

By integrating (3), (4) can be expressed as

$$\mathbf{H} = \sum_{l=1}^{L} g_l \mathbf{a}(\theta_l) \mathbf{b}^H(\tau_l), \tag{5}$$

where $\mathbf{a}(\theta) = \left[A_{m_1}(\theta)\, A_{m_2}(\theta) \cdots A_{m_{M_s}}(\theta)\right]^T$ and $\mathbf{b}(\tau) = \left[e^{-j2\pi\tau f_1}\, e^{-j2\pi\tau f_2} \cdots e^{-j2\pi\tau f_{N_s}}\right]^H$. Let $\mathbf{v}(\theta, \tau) = \mathbf{b}(\tau) \otimes \mathbf{a}(\theta)$ yields the vectorization of $\mathbf{H}$, which called $\mathbf{h}$. The l-th path can be fully characterized by a 3-tuple in the form (g_l, θ_l, τ_l). Therefore, we can determine the mmWave channel as long as 3-tuples for each of the L paths in the mmWave channel are available.

III. Fast-ABS

A. Rationale

As illustrated in Fig. 1, a mobile device has four antenna arrays placed over the four edges. However, currently available mobile devices are restricted to powering only one antenna module at a time due to component cost and power consumption considerations. If an object blocks the received subarray, then the mobile device switches to another subarray and re-scan the best beam direction. Scanning may be invoked persistently among multiple subarrays, exacerbating latency. Therefore, although the use of a large number of subarrays can theoretically provide good coverage, if antenna switching cannot actually be performed with a low beam management overhead, then the function will soon become difficult, becoming a detriment rather than a benefit.

To solve the aforementioned problem, Fast-ABS is proposed on the basis of the preceding rationale. From (5), we observe that although changing subarrays leads to different channel measurements at the receiver, the underlying physical signal paths traversed by each subarray should remain the same and can be defined well by a 3-tuple. Different subarrays in various locations have varying but *fixed* orientations. Therefore, if a receiver can extract the 3-tuple of each L mmWave paths, then the receiver can accurately reconstruct an estimate of the channel for any subarrays. We provide the details of this observation and present its implementation in the succeeding subsections.

B. ToA and AoA between Antenna Arrays

Fig. 2 illustrates how Fast-ABS approaches the goal. Suppose that mmWave wireless signals from the BS to the mobile device traverse two paths. Let the corresponding 3-tuples of the signal paths at array 1 be $(g_1^{[1]}, \theta_1^{[1]}, \tau_1^{[1]})$ and $(g_2^{[1]}, \theta_2^{[1]}, \tau_2^{[1]})$. The signals

Authorized licensed use limited to: National Chiao Tung Univ.. Downloaded on April 26,2022 at 10:09:46 UTC from IEEE Xplore. Restrictions apply.

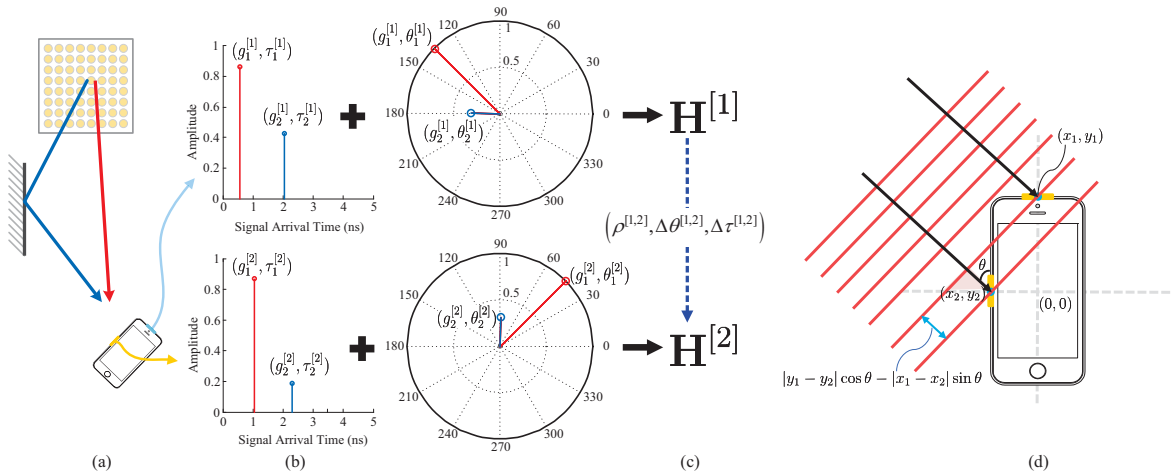

Fig. 2. Rationale behind Fast-ABS: (a) Two subarrays share the same physical paths to reach the mobile device. (b) Measured channel responses show the ToA and AoA of the two paths under both subarrays. (c) Although the two channels look extremely different, we can map the 3-tuples of the paths back to the channels of array 1 to predict the channels of array 2. (d) Diagram of AoA and ToA between two different subarrays.

along the two paths are also received by a different array as shown in Fig. 2(b). In array 2, the AoA of each path is rotated with a fixed angle, but the ToA of each path is varied at different times. Nevertheless, ToA still can be determined from the AoA and the position of the subarray following this proposition.

Proposition 1: Assume that the coordinates of subarrays are central at (x_1, y_1) and (x_2, y_2), as shown in Fig. 2(d). If the AoA of a path to array 2 is θ_l, then the propagation delay time between the two antennas is

$$\Delta\tau_l = |y_1 - y_2|\cos\theta_l - |x_1 - x_2|\sin\theta_l. \tag{6}$$

Proof: The red line through (x_1, y_1) cut out a triangle with the acute angle θ, opposite side $|y_1 - y_2|$, and adjacent side $|y_1 - y_2|\cot\theta$. Then, we obtain the hypotenuse of the (red) triangle as $|y_1 - y_2|\cot\theta - |x_1 - x_2|$. Finally, the propagation delay can be calculated by $\sin\theta(|y_1 - y_2|\cot\theta - |x_1 - x_2|)$, which can be rearranged as the above result. □

Consequently, if we can extract $(\theta_l^{[i]}, \tau_l^{[i]})$ of the paths from array i, then the receiver can infer those for array j. In particular, we have

$$\theta_l^{[j]} \leftarrow \theta_l^{[i]} + \Delta\theta^{[i,j]}, \tag{7a}$$
$$\tau_l^{[j]} \leftarrow \tau_l^{[i]} + \Delta\tau_l^{[i,j]}, \tag{7b}$$

where $\Delta\theta^{[i,j]}$ denotes the angular rotation of array i with respect to (w.r.t.) array j, and $\Delta\tau_l^{[i,j]}$ based on (6) denotes the delay time of array i w.r.t. array j.

C. Gain between Antenna Arrays

In this subsection, we determine the channel gains of the other subarrays for the 3-tuples of the paths. During initial access, the subarray with the maximum signal energy is selected as the primary receive antenna (named as array 1). The loss from hand blockage on antenna gains can reach up to $20 - 25$ dB [4], implying that a subarray without hand blockage shall be selected as the primary receiver antenna. Therefore, we can assume that the 3-tuple of the signal paths extracted from array 1 do not involve hand blockage. Although the underlying propagation paths for the blocked subarray can be different due to coupling and reflection caused by fingers, the detailed properties of this subarray are irrelevant because selecting a blocked subarray should be avoided.

Considering the aforementioned concept, we only need to determine whether the other subarrays are blocked. Such classification can be realized by using a power detector. A power detector can be applied at the output of the (image rejection) bandpass filter. Each subarray is equipped with one power detector and measures power on the basis of a pseudo-omni beam.

Let $\rho^{[i,j]}$ be the power ratio for array j to array i. When the power ratio between subarrays is available, the receiver can infer the complex channel gain for array j via

$$g_l^{[j]} \leftarrow \rho^{[i,j]} g_l^{[i]}. \tag{8}$$

If array j is a hand blockage, then we expect $\rho^{[i,j]}$ to obtain a small value. In such case, array j will not be selected. Each subarray should have its own boresight direction; thus, we can classify the AoA of each path to either be at the front or back of a subarray. If the AoA of a path is at the back of a subarray, then we can disregard its contribution because a loss exceeding 20 dB is observed in this path. For this purpose, we formulate (8) as follows:

$$g_l^{[j]} = \begin{cases} \rho^{[i,j]} g_l^{[i]}, & \theta_l^{[j]} \in \text{boresight of array } j, \\ 0, & \text{otherwise.} \end{cases} \tag{9}$$

D. Antenna Switching and Beam Alignment

Using (7) and (9), we can recreate the channels of array j from (3) as follows:

$$H_m^{[j]}[f_n] = \sum_{l=1}^{L} g_l^{[j]} \cdot A_m(\theta_l^{[j]}) \cdot e^{-j2\pi\tau_l^{[j]} f_n}. \tag{10}$$

Given that the radiation pattern A_m of each beam for array j is known, we can determine the channel conditions of all the beams without conducting a physical scan through the entire space. Using our knowledge of channel conditions and by calculating

$$B_m^{[j]} = \sum_{\forall f_n} |H_m^{[j]}[f_n]|^2, \quad \forall m, j, \tag{11}$$

Authorized licensed use limited to: National Chiao Tung Univ.. Downloaded on April 26,2022 at 10:09:46 UTC from IEEE Xplore. Restrictions apply.

we can predict the candidate beams among all the subarrays. We can keep track of a small set of "good" beams, and quickly switch to the best one before the current beam fails. The beam switching can be performed freely among the subarrays because we have considered all the available beams of multiple subarrays.

From (10), we observe that ToA $\tau_l^{[j]}$ changes the phase of each path at different frequencies. The receiver beam can only focus in one direction at a time because analog beamforming is adopted. That is, the selected beam should be applied to all the subcarriers. Therefore, we infer that the relative ToA $\Delta\tau_l^{[i,j]}$ between arrays i and j is irrelevant in analog beam selection. Accordingly, we introduce the *virtual* channel

$$\widetilde{H}_m^{[j]}[f_n] = \sum_{l=1}^{L} g_l^{[j]} \cdot A_m(\theta_l^{[j]}) \cdot e^{-j2\pi\tau_l f_n}. \tag{12}$$

by assuming that all the subarrays receive path signals simultaneously. This simplification can facilitate the implementation of angle rotation (7a) through a simple table lookup in accordance with the AoAs.

E. Path Parameter Estimation Algorithm

Estimating the ToA, AoA, and gain of multipath from a channel is a critical task in realizing Fast-ABS. This task should be conducted under beam-specific CSI measurements of different beam patterns. From the defination of $\mathbf{h}$, the given set of beam-specific CSI measurements can be modeled as

$$\mathbf{y} = \sum_{l=1}^{L} g_l \mathbf{v}(\theta_l, \tau_l) + \mathbf{z}, \tag{13}$$

where $\mathbf{z}$ is the additive noise vector. The 3-tuples of the paths $(\mathbf{g}, \boldsymbol{\theta}, \boldsymbol{\tau}) = \{(g_l, \theta_l, \tau_l)\}_{l=1}^{L}$ can be estimated by jointly minimizing

$$J(\mathbf{g}, \boldsymbol{\theta}, \boldsymbol{\tau}) = \left\| \mathbf{y} - \sum_{l=1}^{L} g_l \mathbf{v}(\theta_l, \tau_l) \right\|_2^2. \tag{14}$$

We adopt the Newtonized orthogonal matching pursuit (NOMP) algorithm [8] because it exhibits better performance than other state-of-the-art algorithms with lower complexity.

To minimize (14) with low complexity, NOMP uses a detection estimation method for identifying each signal path. NOMP first identifies the strongest signal path, subtracts it from $\mathbf{y}$, and then determines the weak signal path using the residual signal $\mathbf{y}_\mathrm{r} = \mathbf{y} - \hat{g}\mathbf{v}(\hat{\theta}, \hat{\tau})$. Let

$$J_\mathrm{r}(g, \theta, \tau) = \|\mathbf{y}_\mathrm{r} - g\mathbf{v}(\theta, \tau)\|_2^2. \tag{15}$$

The procedure consists of two stages:

1) Coarse detection: Coarse estimates of AoA, ToA, and complex gain are obtained using pre-computed $\{\mathbf{v}(\theta, \tau)\}$

$$(\hat{\theta}, \hat{\tau}) = \underset{\theta\in\boldsymbol{\Theta}, \tau\in\boldsymbol{\Gamma}}{\operatorname{argmax}} |\mathbf{v}^H(\theta, \tau)\mathbf{y}|^2, \tag{16a}$$

$$\hat{g} = \mathbf{v}^H(\hat{\theta}, \hat{\tau})\mathbf{y} / \|\mathbf{v}(\hat{\theta}, \hat{\tau})\|_2^2, \tag{16b}$$

   where $\boldsymbol{\Theta}$ and $\boldsymbol{\Gamma}$ denote the discretized sets of AoAs and ToAs, respectively.

2) Refinement: The estimates are refined using the Newton method:

$$(\hat{\theta}, \hat{\tau}) \leftarrow (\hat{\theta}, \hat{\tau}) - [\nabla^2 J_\mathrm{r}(\hat{g}, \hat{\theta}, \hat{\tau})]^{-1} \nabla J_\mathrm{r}(\hat{g}, \hat{\theta}, \hat{\tau}), \tag{17a}$$

$$\hat{g} \leftarrow \mathbf{v}^H(\hat{\theta}, \hat{\tau})\mathbf{y} / \|\mathbf{v}(\hat{\theta}, \hat{\tau})\|_2^2, \tag{17b}$$

   where $\nabla^2 J_\mathrm{r}$ and ∇J_r denote the Hessian and gradient of J, respectively, with respect to (θ, τ) at the current estimate $(\hat{\theta}, \hat{\tau})$ provided by (16a).

The algorithm is repeated with the residual signal $\mathbf{y}_\mathrm{r}$ to estimate other paths. To improve accuracy, the refinement steps are repeated after each new detection for all the paths in a cyclic manner for a few rounds.

F. Summary

The summary of Fast-ABS is now presented. We assume that an initial beam is established. Thereafter, Fast-ABS, along with the receiver-side beam adjustment, performs as follows. First, a mobile device performs receiver-side beam sweeping on the basis of the data received from an antenna to measure a configured CSI-RS in sequence over a set of receiver beams. The mobile device then extracts 3-tuples for each L paths using the NOMP algorithm. Simultaneously, the other subarrays perform power detection to determine the power ratios between subarrays. Subsequently, the mobile device reconstructs the virtual channels of all the subarrays (12) using the 3-tuples of the paths and the power ratios. Then, we calculate the channel conditions of all the beams $\{B_m^{[j]}\}$ using (11). The mobile device switches to the best beam based on $\{B_m^{[j]}\}$. When the receiver switches to the subarray with the identified beam, the preceding procedure is repeated. Notably, the mobile device also performs beam adjustment during CSI-RS measurements. Therefore, if the switched beam is not the best, then the mobile device can adjust the beam during the beam adjustment procedure.

IV. Simulations and Implementation

We first conduct simulations to evaluate the efficiency of the NOMP algorithm under beam-specific CSI measurements and verify that ToA does not affect the analog beam selection. Next, we implement Fast-ABS on software radios and evaluate its performance via over-the-air (OTA) tests. In the following simulations and experiments, we consider that each array has four antenna elements with a uniform separation of half wavelength. In mmWave systems, exhaustive scan (ES) is a promising method to find the best beam direction with substantial searching latency. Therefore, we regard the result corresponding to ES as an "Oracle" solution. To obtain the performance benchmark, we perform the ES of the azimuth angle with 481 grids in the angular span of $[30°, 150°]$, that is, $0.25°$ spacing per partition. Therefore, we select the peak value of the received SNR (RSNR) value corresponding to the angle as the received angle of the ES.

A. Simulations

The NOMP algorithm can estimate multipath parameters under less beam-specific CSI measurements, which significantly reduces searching latency. Considering the simulation environment with two paths, we utilize four-, three-, and two-beam patterns to obtain beam-specific CSI measurements, that is, $|\mathcal{M}| = 2, 3, 4$. The angular directions of the four-, three-, and two-beam patterns are centralized at $[45°, 75°, 105°, 135°]$, $[50°, 90°, 130°]$, and $[60°, 120°]$, respectively. We consider the two two-path scenarios: one is the line-of-sight (LoS), and the other reflection path is 10 dB (Case 1) and 20 dB (Case 2) weaker than the LoS path (due to reflection loss).

Fig. 3 shows the cumulative distribution function (CDF) of the estimation error of the dominant path, that is, $|\hat{\theta}_1 - \theta_1|$, under different SNRs. The estimation accuracies of all algorithms

Authorized licensed use limited to: National Chiao Tung Univ.. Downloaded on April 26,2022 at 10:09:46 UTC from IEEE Xplore. Restrictions apply.

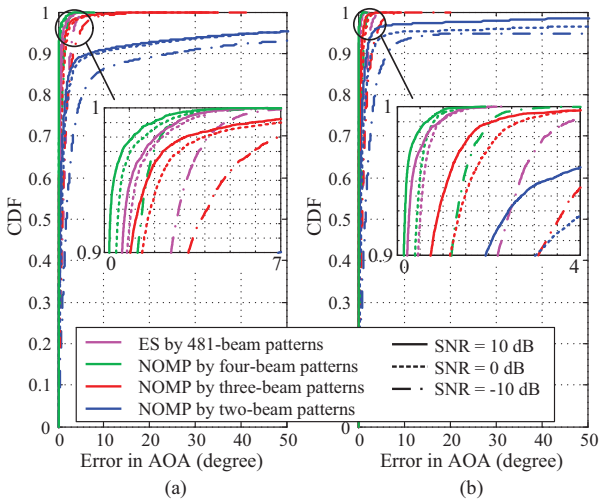

Fig. 3. CDFs of NOMP's AoA estimation errors at different SNRs for (a) Case 1 and (b) Case 2.

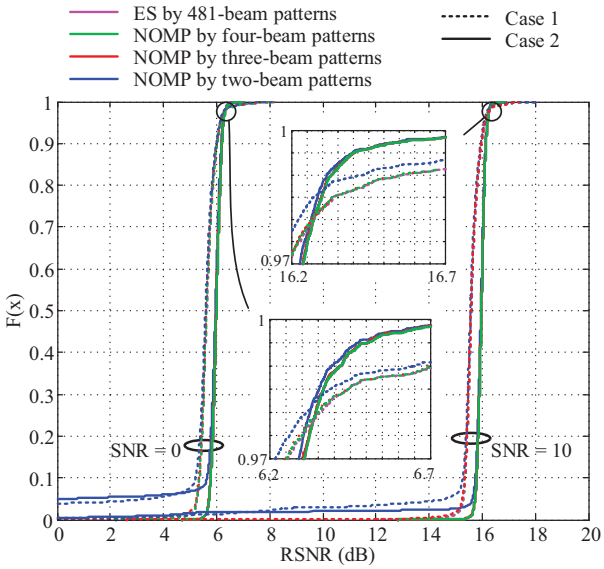

Fig. 4. CDFs of NOMP's RSNRs with respect to ES for Case 1 and Case 2.

improve with the increase in SNR, and the outcome of NOMP improve as the size of beam patterns increases. Comparing the results between Fig. 3(a) and 3(b) indicates that the overall performance under Case 2 is better than that under Case 1. This result is reasonable because, when the path difference reaches 20 dB, we can regard the setting as a single-path channel. We also find that the estimation result of NOMP using four-beam patterns is better than that of ES even under the single-path channel. This result indicates that NOMP exhibits robustness to multipath and produces a high resolution that exceeds $0.25°$.

The RSNR calculated after beamforming is our final performance target and not the estimated angle. Therefore, we present the CDF of RSNR for the concerned methods in Fig. 4. Notably, the beamforming matches the direction of the strongest path when NOMP is used. We find that NOMP with only three- to four-beam patterns present a similar RSNR to ES across all scenarios.

TABLE I
TWO SETS OF SUBARRAY MEASUREMENT RESULTS.

	Array 1		Array 2		Difference
	AoA	RSNR	AoA	RSNR	of AoA
LoS	120.2	28.0	32.5	27.6	88
	128.5	28.8	41.9	28.5	87
	132.0	28.2	43.2	28.7	89
	139.2	28.9	50.0	28.6	89
	143.8	28.4	52.3	28.0	91
NLoS	130.5	11.8	41.1	18.5	89
	134.2	14.9	45.0	18.1	89
	139.0	16.0	50.8	24.2	88

NOMP significantly reduces the latency by nearly 160 times to achieve the same performance.

B. Implementation

Through the above-mentioned simulations, we have verified our proposals that 1) NOMP can be an efficient algorithm to extract the 3-tuple of paths through only three to four probings of beam-specific CSI measurements, and 2) the virtual channel is an effective CSI for beam selection. To verify the feasibility of Fast-ABS, we propose our main rationale that the underlying physical signal paths traversed by each subarray should remain the same. That is, a fixed angular rotation occurs between two arrays on a mobile phone. Toward this end, we implement Fast-ABS on software radios and integrate it into a 5G NR physical layer.

The architecture of our testbed is shown in Fig. 5(a). In the transmitter side, the baseband (BB) signal is first modulated to 4 GHz as an intermediate frequency (IF) signal. Next, the up-converter performs the quadruple operation of the 6 GHz carrier generated by the local oscillator (LO) with a frequency multiplier to obtain the 24 GHz carrier. Finally, a mixer is used to modulate the 4 GHz IF signal with a 24 GHz carrier to generate a 28 GHz radio frequency (RF) signal and use the horn antenna to emanate the RF signal (Fig. 5(b)). The BB signal is based on the 5G NR physical layer with a bandwidth of 100 MHz for a subcarrier spacing of 60 kHz.

In the receiver side, the down converter at the receiver also operates with the LO to obtain the 4 GHz IF signal back. The oscilloscope demodulates the signal to the BB signal. The mobile phone consists of two 4×1 dipole subarrays placed at the edges of the mobile phone (Fig. 5(c)). For our hardware, each receiver antenna element is equipped with an RF chain. Therefore, we use digital beamforming to simulate the equivalent result of the analog beamforming. Notably, we have developed a calibration procedure to achieve the phase coherence of each subarray.

Our testbed can receive signals from the two arrays simultaneously. Thus, whether a fixed angular rotation occurs between two arrays can be easily verified. Fig. 5(d) depicts the effective angular range of the two subarrays. In the LoS scenario, the BS is placed at the protractor and we record every measurement result per $6°$ change in position. In the NLoS scenario, the horn antenna doesn't transmit a signal directly to the receiving direction but utilizes an iron plate to simulate a reflection path as shown in Fig. 5(e). We rotate the iron plate to obtain different reflection paths. Table I shows the corresponding results, where the AoAs of the two arrays are extracted simultaneously via NOMP. We observe that approximately $90°$ angular rotation occurs between the two arrays for LoS and NLoS scenarios. Consequently, a specific

Authorized licensed use limited to: National Chiao Tung Univ.. Downloaded on April 26,2022 at 10:09:46 UTC from IEEE Xplore. Restrictions apply.

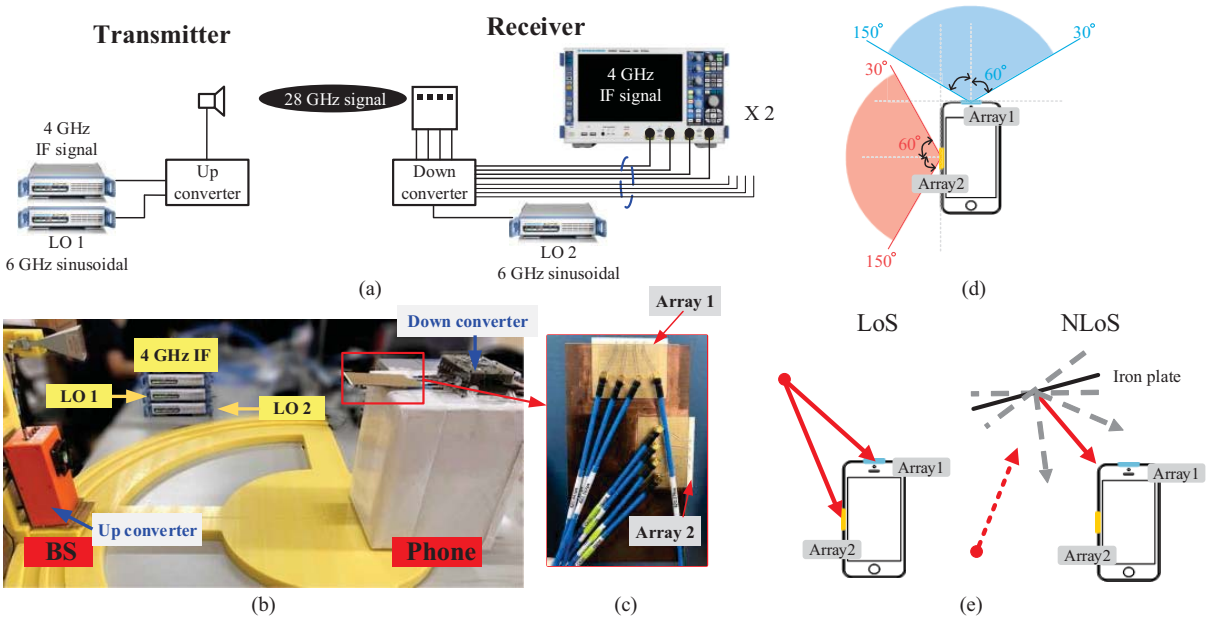

Fig. 5. (a) Architectural schematics of mmWave testing platform. (b) mmWave testing platform (actual scenario). (c) Two 4×1 dipole arrays. (d) Beam receiving effective range. (e) Environment of LoS and NLoS.

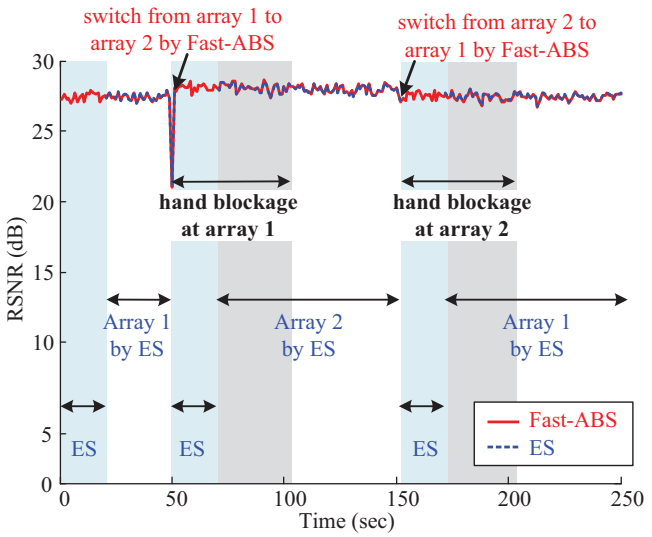

Fig. 6. RSNR trajectory during Fast-ABS process over the mmWave testing platform. Corresponding RSNRs of Fast-ABS and ES are plotted by red and blue dotted lines, respectively.

range of angle conversion exists between the two subarrays, which verify Fast-ABS is feasible.

The RSNR of Fast-ABS achieved with an ≈ 250 second trajectory is illustrated in Fig. 6. The figure shows some links drop due to penetration loss through hand blockage, and other links remain due to array switching. ES switches antennas in turn and re-scan the best beam with 481-beam patterns. To observe the array switching state under hand blockage, we block the two arrays sequentially during the OTA test. We observe that, during array switching, ES spends considerable time to change the array, data cannot be received during scanning. Meanwhile, no time is required for beam scanning because Fast-ABS can switch the array and beam rapidly. After switching the array, the RSNR of Fast-ABS remains the same as that of ES at around 27 dB.

V. Conclusions

Developing a fast and efficient operation that can determine the best subarray and beam direction with power, complexity, and latency constraints is challenging. In this study, we presented Fast-ABS, which can use only one subarray for the reception to predict the best beam of other antenna arrays. Compared with existing solutions, Fast-ABS has the advantages of efficient and seamless connectivity under hand blockage. A series of experimental results showed that Fast-ABS can achieve a performance close to that of an "Oracle" solution because it can instantaneously identify the best beam of other subarrays even in complex NLoS scenarios.

References

[1] Apple Inc. (Cupertino, CA, US), "Electronic devices with millimeter wave antennas and metal housings," U.S. Patent 20 190 214 708.

[2] *Spherical Coverage of Realistic Design*, document R4-1712381, 3GPP TSG-RAN WG4 Meeting #85, Qualcomm, Reno, NV, USA Std., Nov./Dec. 2017.

[3] *UE Spherical Coverage at mmWave 28 GHz*, document R4-1802868, 3GPP TSG-RAN WG4 #86, Sony, Athens, Greece Std., Feb./Mar. 2018.

[4] V. Raghavan, M.-L. Chi, M. A. Tassoudji, O. H. Koymen, and J. Li, "Antenna placement and performance tradeoffs with hand blockage in millimeter wave systems," *IEEE Trans. Commun.*, vol. 67, no. 4, pp. 3082–3096, 2019.

[5] J. Mo, B. L. Ng, S. Chang, P. Huang, M. N. Kulkarni, A. Alammouri, J. C. Zhang, J. Lee, and W.-J. Choi, "Beam codebook design for 5G mmWave terminals," *IEEE Access*, vol. 7, pp. 98 387–98 404, 2019.

[6] X. Lin, J. Li, R. Baldemair, J.-F. T. Cheng, S. Parkvall, D. C. Larsson, H. Koorapaty, M. Frenne, S. Falahati, A. Grovlen *et al.*, "5G new radio: Unveiling the essentials of the next generation wireless access technology," *IEEE Commun. Mag.*, vol. 3, no. 3, pp. 30–37, 2019.

[7] A. Alammouri, J. Mo, B. L. Ng, J. C. Zhang, and J. G. Andrews, "Hand grip impact on 5G mmWave mobile devices," *IEEE Access*, vol. 7, pp. 60 532–60 544, 2019.

[8] B. Mamandipoor, D. Ramasamy, and U. Madhow, "Newtonized orthogonal matching pursuit: Frequency estimation over the continuum," *IEEE Trans. Signal Process.*, vol. 64, no. 19, pp. 5066–5081, 2016.

Authorized licensed use limited to: National Chiao Tung Univ.. Downloaded on April 26,2022 at 10:09:46 UTC from IEEE Xplore. Restrictions apply.